THE JOURNAL OF PHYSICAL CHEMISTRY C
Article
pubs.acs.org/JPCC

Panchromatic Light Harvesting and Hot Electron Injection by Ru(II) Dipyrrinates on a TiO_2 Surface

Guocan Li,[†] Ke Hu,[‡] Chongyue Yi,[†] Kenneth L. Knappenberger, Jr.,*[,†] Gerald J. Meyer,*[,‡]
Serge I. Gorelsky,*[,§] and Michael Shatruk*[,†]

[†]Department of Chemistry and Biochemistry, Florida State University, Tallahassee, Florida 32306, United States

[‡]Department of Chemistry and Materials Science and Engineering, Johns Hopkins University, 3400 North Charles Street, Baltimore, Maryland 21218, United States

[§]Centre for Catalysis Research and Innovation, Department of Chemistry, University of Ottawa, Ottawa, Ontario K1N 6N5, Canada

S *Supporting Information*

ABSTRACT: Three Ru(II) dipyrrinate complexes, $[Ru(bpy)_2(3\text{-TDP})](PF_6)$ (**1**), $[Ru(H_2dcbpy)(Hdcbpy)(3\text{-TDP})]$ (**2**), and $[Ru(H_2dcbpy)(Hdcbpy)(TPADP)]$ (**3**) (bpy = 2,2′-bipyridine; dcbpy = 4,4′-dicarboxylato-2,2′-bipyridine; 3-TDP = 3-thienyl-dipyrrinate; TPADP = triphenylamino-dipyrrinate), have been synthesized and characterized by electrochemical and photophysical methods as well as by theoretical electronic structure calculations on the DFT level. The complexes exhibit panchromatic light harvesting due to complementary ligand-based absorption around 450 nm and metal-to-ligand charge transfer (MLCT) absorption around 530 nm. Complexes **2** and **3** have been investigated as potential sensitizers for the dye-sensitized solar cell (DSSC). Time-dependent DFT calculations reveal the preferential localization of an excited-state electron on the H_2dcbpy ligands, leading to a favorable scenario for electron injection from these anchoring ligands into TiO_2. Solution-phase transient absorption spectroscopy was used to follow the excited state dynamics of methyl-ester derivatives of **2** and **3**. Excitation with a 400-nm laser pulse resulted in two bleaches centered at 460 and 540 nm and corresponding to the ligand-based and MLCT transitions, respectively. A rapid 2 ps loss of the ligand based bleach corresponded with a growth of the MLCT bleach that were interpreted as the result of vibrational relaxation between metal-centered and ligand-centered frontier orbitals. The electron-injection kinetics were studied on dyes **2** and **3** anchored on the TiO_2 surface. The excited state electron-injection yield and incident photon-to-current efficiency were dramatically suppressed by addition of *tert*-butylpyridine (TBP), indicating that the lowest excited state was positioned close in energy to the TiO_2 acceptor states. Nevertheless, the injection yield measured with 416-nm excitation was less sensitive to the TBP concentration than that measured with 532-nm excitation, thus suggesting the possibility of hot-electron injection from the upper excited states generated by the ligand-based excitations. Based on the findings of this study, a pathway is proposed for improving the electron-injection yield of Ru-dipyrrinate dyes and increasing the power-conversion efficiency of the DSSC incorporating these dyes.

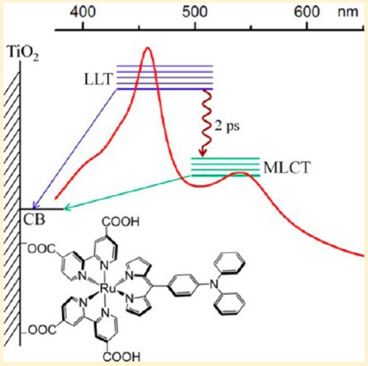

INTRODUCTION

The growing energy demand of mankind and depletion of fossil fuels stipulate the need for environmentally friendly and sustainable energy technologies. In this vein, solar energy has been the focus of extensive research efforts for many years. In particular, dye-sensitized solar cells (DSSCs) have been explored as a promising technology to provide robust energy-conversion solutions adaptable to various rigid and flexible substrates.[1−4] The key component in the DSSC device is the dye that harvests sunlight, injects electrons into wide-band gap semiconductor (usually TiO_2), and then oxidizes a redox mediator present in electrolyte solution.[5] Ru−polypyridyl complexes incorporating thiocyanate ligands, such as $[Ru(H_2dcbpy)_2(NCS)_2]$ (**N3**; dcbpy = 4,4′-dicarboxylato-2,2′-bipyridine),[6] $(Bu_4N)_2[Ru(Hdcbpy)_2(NCS)_2]$ (**N719**),[7] and $(Bu_4N)_3[Ru(Htctpy)(NCS)_3]$ (**N749**; tctpy = 2,2′:6′,2″-terpyridyl-4,4′,4′-tricarboxylate),[8] are among the most widely used DSSC dyes due to their strong absorptivity in the visible range and favorable redox potentials that facilitate the charge injection.[9] A number of recent studies, however, have focused on developing alternative NCS-free Ru dyes[10−14] to address stability problems associated with the lability of the NCS^- ligands.[15] In particular, chelating ligands, such as phenyl-pyridine,[16] phenyl-bipyridine,[17] and pyridine-pyrazole,[18] have been shown to act as effective alternatives to the monodentate NCS^-.

We have recently reported a detailed investigation of Ru complexes with chelating dipyrrinates and demonstrated their viability as DSSC sensitizers.[19,20] Dipyrrins themselves are strongly absorbing molecules that are well-known as precursors

Received: May 11, 2013
Revised: July 21, 2013
Published: July 30, 2013

dx.doi.org/10.1021/jp404670z | *J. Phys. Chem. C* 2013, 117, 17399−17411

to porphyrins and components of widely used BODIPY complexes.[21] Their Ru complexes exhibit two strong (and complementary) absorption bands in the visible range.[22,23] The higher-energy band has been attributed to a combination of intramolecular ligand-to-ligand charge-transfer and dipyrrin $\pi-\pi^*$ transitions, herein referred to as ligand-localized transitions (LLT), while the lower-energy band was assigned as metal-to-ligand charge-transfer (MLCT) transitions. Thus, one can expect that these complexes will act as panchromatic DSSC sensitizers with excellent light-harvesting properties. Increasing the molar absorptivity of the sensitizer should allow the use of thinner layers of mesoporous TiO_2 or other morphologies, such as nanowires, that have inherently low surface areas. This advance, in turn, will facilitate the exploration of fast outer-sphere redox mediators, such as Co^{III}/Co^{II} and Fc^+/Fc (Fc = ferrocene), as alternatives to the ubiquitous I_3^-/I^- redox couple.

Thus far, the efficiency of the DSSC prepared with Ru—dipyrrinate dyes turned out to be quite low, despite their excellent absorptivity.[19] Nevertheless, we achieved appreciable photocurrent densities, which suggest thermodynamically favorable electron injection from the excited state(s) of the dye into TiO_2. Further studies are necessary to understand the fundamental mechanism underlying the excitation and electron-injection processes in these dyes and improve their DSSC performance.

Herein we report detailed optical and electron-injection studies of Ru dipyrrinates, $[Ru(bpy)_2(3\text{-TDP})](PF_6)$ (**1**), $[Ru(H_2dcbpy)(Hdcbpy)(3\text{-TDP})]$ (**2**), and $[Ru(H_2dcbpy)(Hdcbpy)(TPADP)]$ (**3**) (bpy = 2,2′-bipyridine; 3-TDP = 3-thienyl-dipyrrinate; TPADP = triphenylamino-dipyrrinate) (Scheme 1). Complexes **1** and **2** bear a 3-thienyl substituent at the meso-position of dipyrrin (DP), and **3** contains a triphenylamine (TPA) substituent at the same position. Time-resolved spectroscopic studies in solution and investigation of dyes on TiO_2 surface, supplemented by DFT calculations, elucidate the influence of substituents on the dipyrrinate and bipyridine ligands on the light-harvesting properties and excited-state dynamics of these complexes and identify pathways to the successful implementation of Ru—dipyrrinate dyes in the DSSC.

Scheme 1. Molecular Structures of Ru(II) Dipyrrinates Studied in This Work

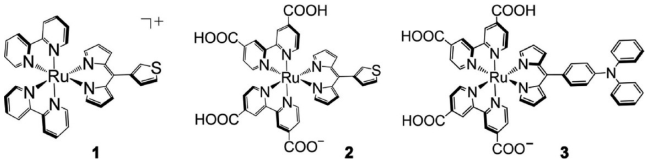

EXPERIMENTAL SECTION

Physical Measurements. ^1H NMR spectra were measured on Bruker 600 MHz spectrometer. Chemical shifts were referenced to the signals of residual protons in deuterated solvents (7.26 ppM in $CDCl_3$ and 3.31 ppm in CD_3OD).[24] Electrospray ionization mass spectra (ESI-MS) were acquired on a Beckman Coulter System Gold HPLC BioEssential with Binary Gradient 125S pump and a UV/vis 166 analytical detector. Electronic absorption (UV—vis) spectra were collected in the 250—800 nm range on a Varian Cary 50 spectrophotometer. A steady-state photoluminescence (PL) spectrum was obtained with a Spex Fluorolog fluorimeter consisting of a single excitation monochromator (1681) optically coupled to a 450 W Xe arc lamp. Detection was achieved by a double detection monochromator (1682) with a GaAs photomultiplier tube (Hamamatsu). For 77 K PL measurement, an argon prepurged solution sample was put into an NMR tube and immersed in liquid nitrogen in a coldfinger. The PL response was detected at a right angle to the excitation beam.

Electrochemistry. Cyclic voltammograms (CV) were recorded on a CH Instruments 600D electrochemical analyzer at the sweep rate of 0.100 $V\cdot s^{-1}$, with 0.100 M $(Bu_4N)PF_6$ electrolyte solution, Pt working electrode, and Ag^+(0.010 M $AgNO_3$)/Ag reference electrode. All of the potentials initially were referenced to the standard Fc^+/Fc couple (Fc = ferrocene). Fc was added as an internal standard upon completion of each CV experiment. The redox potentials reported in this work have been converted to the normal hydrogen electrode (NHE), assuming that the Fc^+/Fc couple has a redox potential of +0.630 V vs NHE in acetonitrile.[25]

Syntheses. All reactions were performed in an inert N_2 atmosphere using standard Schlenk techniques, unless noted otherwise. All reagents were purchased from Aldrich and used as received, except for pyrrole (Alfa Aesar) which was distilled prior to use. 5-(2-Thienyl)-4,6-dipyrromethane,[26] 4,4′-bis-(methoxycarbonyl)-2,2′-bipyridine (dcmb),[27] $[(p\text{-cymene})RuCl_2]_2$,[28] *N,N*-(diphenylamino)benzaldehyde,[29] $[Ru(bpy)_2(3\text{-TDP})]PF_6$ (**1**),[20] and $[Ru(dcmb)_2(3\text{-TDP})]PF_6$ (**2a**)[20] were prepared according to reported procedures. Anhydrous commercial solvents were additionally purified by passing through a double-stage drying/purification system (Glass Contour Inc.).

$[Ru(H_2dcbpy)(Hdcbpy)(3\text{-TDP})]$ (2). A solution containing **2a** (41 mg, 0.040 mmol), 3 mL of Et_3N, 3 mL of H_2O, and 9 mL of DMF was heated at reflux for 18 h. After cooling to r.t., the solvent was evaporated to dryness under reduced pressure, and 30 mL of CH_2Cl_2 was added to dissolve the unreacted starting material which was removed by filtration subsequently. The obtained filter cake was washed with diethyl ether (3 × 10 mL) and dried under vacuum to afford 28 mg of black solid. Yield = 85%. ^1H NMR (CD_3OD, 600 MHz), δ, ppm: 9.02 (d, J = 5.4 Hz, 4H), 8.08 (d, J = 5.9 Hz, 2H), 7.96 (d, J = 5.8 Hz, 2H), 7.89 (dd, J = 5.9, 1.7 Hz, 2H), 7.79 (dd, J = 5.8, 1.7 Hz, 2H), 7.55 (dd, J = 3.0, 1.3 Hz, 1H), 7.51 (dd, J = 5.0, 3.0 Hz, 1H), 7.25 (dd, J = 5.0, 1.2 Hz, 1H), 6.78 (dd, J = 4.4, 1.3 Hz, 2H), 6.39 (t, J = 1.5 Hz, 2H), 6.30 (dd, J = 4.4, 1.5 Hz, 2H). HR-ESI-MS: m/z = 815.05070 (calcd. for $[Ru(H_2dcbpy)_2(3\text{-TDP})]^+$: 815.04981). Elem. analysis: calcd. (found) for $RuSO_{12}N_6C_{37}H_{32}$ ($\mathbf{1}\cdot 4H_2O$), %: C, 50.17 (49.84); H, 3.64 (3.75); N, 9.49 (9.71).

TPA—dipyrromethane. Freshly distilled pyrrole (6 mL) was added to 1.00 g (3.66 mmol) of *N,N*-(diphenylamino)-benzaldehyde in a 50-mL Schlenk flask. The solution was degassed for 15 min, and 84 μL of trifluoroacetic acid (TFA) was added. The mixture was stirred at r.t. for 2 h, and then 0.5 mL of Et_3N was added to quench the reaction. After addition of 30 mL of CH_2Cl_2, the mixture was washed with water (3 × 30 mL). The organic phase was collected and dried over anhydrous $MgSO_4$. The solvent and excess pyrrole were removed under reduced pressure, and the crude product was charged on a silica gel column (4 cm × 18 cm). Using CH_2Cl_2:hexanes (1:1, v/v) as eluent, the first colorless band was collected and evaporated to dryness under vacuum to produce 1.20 g of brownish oil. Yield = 84%. ^{1}H NMR ($CDCl_3$, 600 MHz), δ, ppm: 7.93 (s, 2H), 7.29−7.20 (m, 4H), 7.12−7.05 (m, 6H), 7.05−6.97 (m, 4H), 6.74−6.66 (m, 2H), 6.22−6.13 (m, 2H), 5.95 (s, 2H), 5.42 (s, 1H). ^{13}C NMR ($CDCl_3$, 151 MHz), δ, ppm: 147.89, 146.78, 136.26, 132.82, 129.37, 129.25, 124.40, 124.05, 122.93, 117.32, 108.58, 107.29, 77.16, 43.57.

[(*p*-Cymene)Ru(TPADP)Cl]. A solution of *p*-chloranil (260 mg, 1.06 mmol) in 10 mL of anhydrous THF was added dropwise to a solution of TPA−dipyrromethane (400 mg, 1.03 mmol) in 10 mL of anhydrous THF. The mixture was stirred for 6 h at r.t. The solvent was removed under reduced pressure, and the crude product was added to a 100 mL Schlenk flask containing 315 mg (0.520 mmol) of $[(\text{p-cymene})_2RuCl_2]_2$. After addition of 1 mL of Et_3N and 30 mL of anhydrous MeCN, the mixture was heated at reflux for 12 h. The reaction was cooled to r.t. and filtered through Celite, and the filtrate was evaporated to dryness under reduced pressure. The crude product was loaded on a silica gel column (2.5 cm × 20 cm) and washed with CH_2Cl_2:MeOH eluent (50:1, v/v). A bright-red band was collected and evaporated to dryness to afford 345 mg of red powder. Yield = 51%. ^{1}H NMR ($CDCl_3$, 600 MHz), δ, ppm: 8.03−7.99 (m, 2H), 7.33−7.25 (m, 6H), 7.20−7.15 (m, 4H), 7.10−7.04 (m, 4H), 6.76 (dd, 2H, J = 4.3, 1.3 Hz), 6.50 (dd, 2H, J = 4.3, 1.4 Hz), 5.32−5.25 (m, 4H), 2.43 (hept, 1H, J = 6.9 Hz), 2.22 (s, 3H), 1.07 (d, 6H, J = 7.0 Hz). ^{13}C NMR ($CDCl_3$, 151 MHz), δ, ppm:154.7, 148.4, 147.6, 146.8, 135.5, 131.7, 131.1, 129.5, 125.1, 123.5, 121.3, 118.3, 102.2, 100.4, 85.0, 84.7, 30.7, 29.7, 22.2, 18.7. HR-ESI-MS: m/z = 622.17974 (calcd. for $[(\text{p-cymene})Ru(TPADP)]^+$: 622.17962).

[Ru(dcmb)$_2$(TPADP)]PF$_6$ (3a). A mixture of [(*p*-cymene)-Ru(TPADP)Cl] (190 mg, 0.29 mmol), dcmb (236 mg, 0.87 mmol), $AgNO_3$ (53 mg, 0.31 mmol), and 30 mL of anhydrous MeOH was heated at reflux for 16 h in the dark. After cooling to r.t., the reaction mixture was concentrated to ∼5 mL under reduced pressure and filtered through a fine porosity frit to remove the excess of dcmb and the AgCl byproduct. To the filtrate was added a solution of NH_4PF_6 (110 mg, 0.67 mmol) in 2 mL of MeOH, and the mixture was stirred vigorously for 1 h to complete the anion exchange. The precipitated product was recovered by filtration, washed with diethyl ether (3 × 10 mL), and dried under vacuum to afford 206 g of **3a** as black powder. Yield = 61%. ^{1}H NMR ($CDCl_3$, 600 MHz), δ, ppm: 8.90 (d, 2H, J = 1.6 Hz), 8.88 (d, 2H, J = 1.6 Hz), 8.01−7.96 (m, 4H), 7.93−7.86 (m, 4H), 7.33−7.28 (m, 4H), 7.25−7.21 (m, 2H), 7.19−7.15 (m, 4H), 7.10−7.05 (m, 4H), 6.81 (dd, 2H, J = 4.4, 1.5 Hz), 6.30 (dd, 2H, J = 4.4, 1.5 Hz), 6.26−6.24 (m, 2H), 4.04 (s, 6H), 4.01 (s, 6H). ^{13}C NMR ($CDCl_3$, 151 MHz), δ, ppm: 164.2, 158.3, 157.5, 152.6, 152.4, 148.7, 148.3, 147.5, 137.6, 137.0, 136.2, 133.2, 132.6, 131.9, 131.7, 129.6, 126.8, 125.9, 125.2, 123.8, 123.2, 122.8, 121.1, 118.7, 77.2, 53.6, 53.5. HR-ESI-MS: m/z = 1032.22912 (calcd. for $[Ru(dcmb)_2(TPADP)]^+$: 1032.22948). Elem. analysis: calcd. (found) for $RuPF_6O_{8.5}N_7C_{55}H_{45}$ (**3a**·$0.5H_2O$), %: C, 55.70 (55.44); H, 3.82 (3.88); N, 8.27 (8.39).

[Ru(bpy)$_2$(TPADP)](PF$_6$) (3b). Complex **3b** was prepared in the same fashion as **3a** using bpy instead of dcmb as the starting material. Yield = 64%. ^{1}H NMR ($CDCl_3$, 600 MHz), δ, ppm: 8.33 (dd, 4H, J = 7.9, 3.6 Hz), 7.89−7.85 (m, 6H), 7.70 (d, 2H, J = 5.4 Hz), 7.31−7.27 (m, 10H), 7.17 (d, 4H, J = 8.0 Hz) 7.09−7.06 (m, 4H), 6.79 (d, 2H, J = 4.2 Hz), 6.38 (s, 2H), 6.32 (d, 2H, J = 4.4 Hz). ^{13}C NMR ($CDCl_3$, 151 MHz), δ, ppm: 158.1, 157.4, 151.9, 150.9, 148.9, 148.3, 147.5, 136.2, 136.1, 135.6, 131.8, 129.5, 126.9, 126.3, 125.0, 123.6, 123.4, 121.4, 118.2. HR-ESI-MS: m/z = 800.20780 (calcd. for $[Ru(bpy)_2(TPADP)]^+$: 800.20757).

[Ru(H$_2$dcbpy)(Hdcbpy)(TPADP)] (3). This complex was prepared starting from **3a** (40 mg, 0.034 mmol), in the manner similar to that described for the preparation of **2**. Yield = 80% (26 mg). ^{1}H NMR (CD_3OD, 600 MHz), δ, ppm: 9.06−9.01 (m, 4H), 8.11 (d, 2H, J = 5.8 Hz), 7.98 (d, 2H, J = 5.9 Hz), 7.90 (dd, 2H, J = 5.9, 1.7 Hz), 7.81 (dd, 2H, J = 5.9, 1.7 Hz), 7.34−7.26 (m, 6H), 7.16−7.12 (m, 4H), 7.11−7.03 (m, 4H), 6.74 (dd, 2H, J = 4.4, 1.1 Hz), 6.41−6.37 (m, 2H), 6.31 (dd, 2H, J = 4.4, 1.5 Hz). HR-ESI-MS: m/z = 976.17041 (calcd. for $[Ru(H_2dcbpy)_2(TPADP)]^+$: 976.16688). Elem. analysis: calcd. (found) for $RuO_{11}N_7C_{51}H_{41}$ (**2**·$3H_2O$), %: C, 59.53 (59.26); H, 4.02 (3.83); N, 9.53 (9.39).

Theoretical Calculations. Density functional theory (DFT) calculations were performed with the Gaussian 09 package,[30] using the B3LYP hybrid functional[31,32] and the DZVP basis set[33] for Ru and the TZVP basis set[34] for the other elements, within spin-restricted molecular orbital (MO) model. The starting geometry for complex **1** was taken from the refined crystal structure parameters.[20] Calculations for complexes **2** and **3** were performed by adding carboxylic acid functionalities (−COOH) to bpy ligands of **1** as well as the TPA substituent in the case of **3**. All geometries were optimized in the ground state, without symmetry restraints, using the polarizable continuum model of solvation (PCM) with acetonitrile as a solvent to include solute−solvent interaction effects. Time-dependent (TD) DFT calculations in solution (using the same PCM model) were carried out on the optimized geometries. The UV−vis spectra were simulated with the SWizard program, revision 4.6,[35,36] using the Gaussian functions with the half-bandwidths, $\Delta_{1/2}$, of 3000 cm^{-1}. Atomic/fragment contributions to the molecular orbitals were calculated using the AOMix software.[35,37]

Solution-Phase Transient Absorption Spectroscopy. Femtosecond time-resolved transient absorption (TA) pump−probe experiments were performed using a 1-kHz regeneratively amplified Ti:sapphire laser system that delivered 800-μJ pulse energies centered at 800 nm. The duration of the amplified pulse was typically ∼90 fs, and the pulse was characterized by frequency-resolved optical gating pulse diagnostics. The amplified laser output was frequency doubled to generate 400-nm light (200 μJ/pulse), which was attenuated and used as the excitation pump pulse. Excitation pulse energies used here ranged from 300 nJ/pulse to 1.0 μJ/pulse. A small portion (4%) of the fundamental laser output was passed through a sapphire plate to generate the continuum probe pulse that typically extended from 450 to 850 nm. The pump−probe time delay was controlled using a retroreflecting mirror mounted on a motorized linear translation stage (Newport). Both pulses were spatially overlapped in the sample−laser interaction region. Differential absorption of the probe was measured as a function of the time delay between the pump and probe by mechanically chopping the pump pulse at 500 Hz. Here, the probe was spectrally dispersed on a silicon diode array to generate a wavelength-resolved differential absorption spectrum that spanned from 450 to 800 nm. Data were acquired for 2 s at each pump−probe delay. The instrument response time (∼150 fs) was determined from the nonresonant response of the pump and probe pulses in solvent. The full dynamic range of the measurements extended from 10 ps

Scheme 2. Synthesis of Complexes 1–3: (a) [(*p*-cymene)$RuCl_2$]$_2$, Et_3N, MeCN, Reflux, 12 h; (b) bpy, $AgNO_3$, NH_4PF_6, MeOH, Reflux, 16 h; (c) dcmb, $AgNO_3$, NH_4PF_6, MeOH, Reflux, 16 h; (d) Et_3N/H_2O/DMF = 1:1:3 (v/v/v), Reflux, 18 h

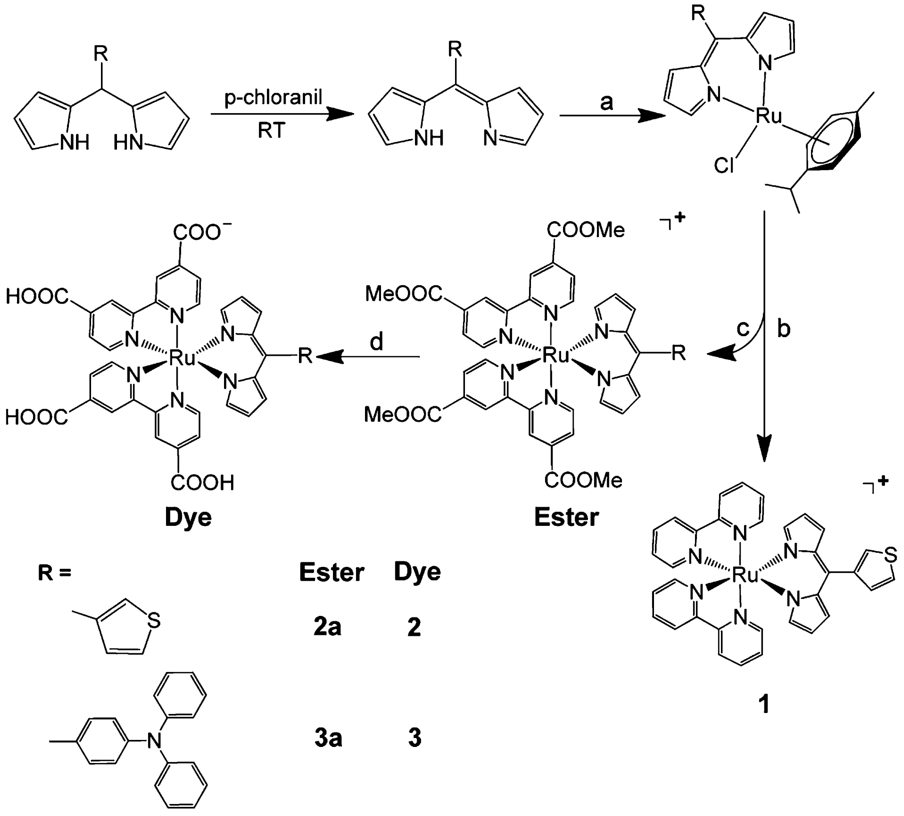

before to 3.2 ns after time zero. Data fitting used in this work was similar to previously published methods.[38] Temporal integration of bleach and excited state absorption peaks measured in the TA spectrum provided electronic relaxation kinetic traces. The transient data were fit with an in-house program that uses an iterative least-squares approach. The best fits were obtained using either single- or multiexponential decay function, which accounted for relaxation time constants

$$S(t) = G(t)^{*} \sum A_n \exp\left(\frac{-t}{\tau_n}\right) \tag{1}$$

where $G(t)$ is a Gaussian function that accounts for the instrument response, t is the pump–probe delay time, A_n is the amplitude coefficient that describes the relative contribution from the nth relaxation component to the total time-dependent signal, and τ_n is the corresponding time constant.

Studies of Dyes on TiO_2 Surface. *Substrate Preparation.* Mesoporous nanocrystalline TiO_2 thin films were prepared as previously described.[39] Briefly, TiO_2 was prepared by acid hydrolysis of Ti(*i*-OPr)$_4$ (Aldrich, 97%) using a sol–gel technique. The TiO_2 was cast onto the transparent FTO (fluorine-doped tin oxide) conductive substrate (Hartford Glass 15 Ω/cm^2) by a doctor blade (~5 μm thick; Scotch tape was employed as the spacer) and annealed at 450 °C for 30 min under constant oxygen flow. The films obtained were immersed in 40 mM $TiCl_4$ aqueous solution at 70 °C for 30 min and rinsed with deionized water. The TiO_2 thin films were sintered again under the same conditions as described above. The films as prepared were immersed in an EtOH solution of the dye (~3 × 10^{-4} M) for time periods of hours to days, then rinsed with EtOH and MeCN, and diagonally positioned in a standard 1 cm^2 quartz cuvette containing 0.5 M solution of $LiClO_4$ in MeCN. The electrolyte solutions were purged with Ar gas for at least 30 min prior to experiments.

Spectroelectrochemistry. Spectroelectrochemistry was carried out in a standard three-electrode cell with a TiO_2 thin-film working electrode, a Pt disk counter electrode, and an Ag/AgCl reference electrode (Bioanalytical Scientific Instruments, Inc.) in a 0.5 M solution of $LiClO_4$ in MeCN, at variable concentrations of *tert*-butylpyridine (TBP). UV–visible absorption measurements were obtained on a Varian Cary 50 spectrophotometer at room temperature. A potentiostat (BAS model CV-50W) was employed, and the applied potential was held until a steady state absorption that was invariant in time was achieved. The typical waiting time was 2–3 min. The Fc^+/Fc half-wave potential was measured at room temperature before and after each experiment and used as an external standard to calibrate the reference electrode. All reported potentials have been converted to the NHE scale as described above.

Transient Absorption Spectroscopy. Nanosecond TA measurements were obtained with an apparatus similar to the one previously described.[39] The samples were excited by a Q-switched, pulsed Nd:YAG laser (Quantel USA (BigSky) Brilliant B; 5–6 ns full width at half-maximum, 1 Hz, ~10 mm in diameter) at 532 nm (frequency doubled) or 416 nm (H_2 Raman shifter with 355 nm laser light) directed at 45° to the film surface. A Glan-Taylor polarizer was employed in the laser path to attenuate the pulse fluence. A 150 W xenon arc lamp coupled to a 1/4 m monochromator (Spectral Energy, Corp. GM 252) served as the probe beam (Applied Photophysics) that was aligned orthogonally to the excitation light. For detection at sub-100 μs time scales the lamp was

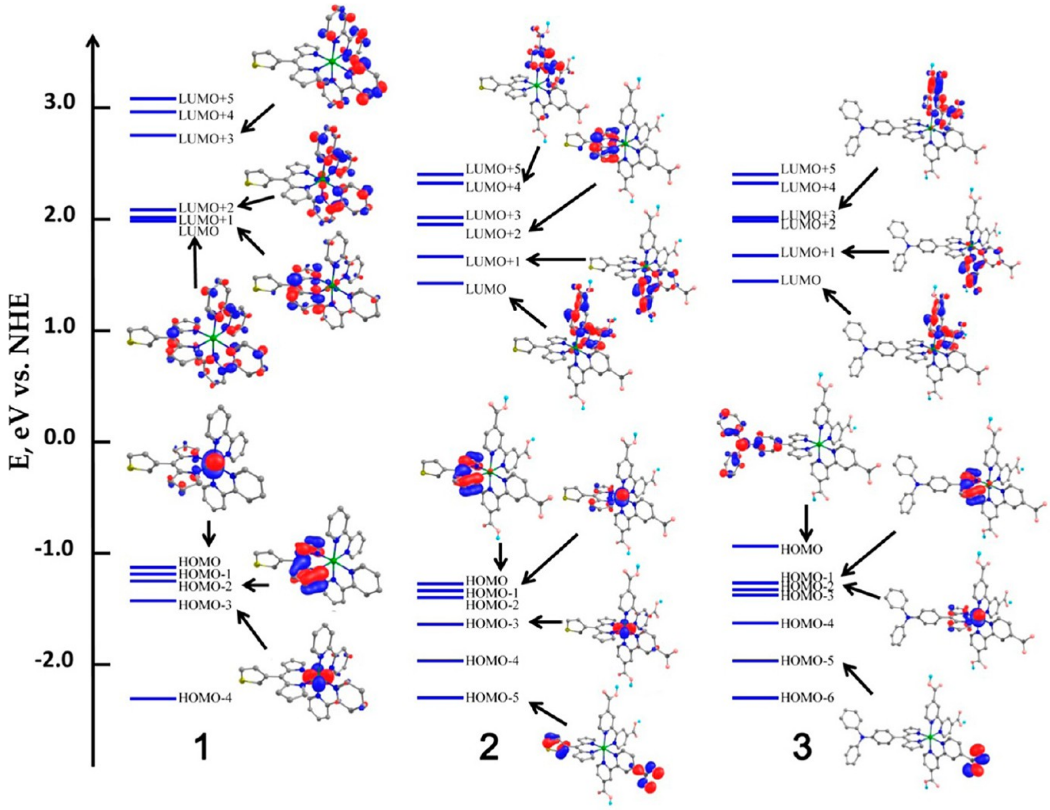

Figure 1. Selected frontier molecular orbitals of **1**, **2**, and **3**. Isosurface contour values are 0.05 a.u. H atoms are omitted for clarity except for the ones on carboxylic acid groups. Color scheme: Ru = green, S = yellow, O = pink, N = blue, C = gray, and H = cyan.

pulsed. Detection was achieved with a monochromator (Spex 1702/04) optically coupled to an R928 photomultiplier tube (Hamamatsu). Transient data were acquired on a computer-interfaced digital oscilloscope (LeCroy 9450, Dual 350 MHz) with 2.5 ns resolution terminated at 50 Ω for sub-100 μs; for longer time scales, the signal was terminated with a 10 kΩ resistor and bandwidth limited at 80 MHz. Approximately 150−250 laser pulses were typically averaged for each single wavelength measurement to achieve satisfactory signal-to-noise ratios. Kinetic data fitting and spectral modeling were performed in Origin 8, and least-squares error minimization was accomplished using the Levenberg−Marquardt iteration method.

Incident Photon to Current Efficiency (IPCE). A two-electrode cell was employed with sensitized TiO_2/FTO as the working electrode and Pt wire as the counter electrode. The working electrode was illuminated through the backside of the FTO slide using a 150 W xenon arc lamp (Spectra-Physics) coupled to a 1/4 m monochromator (Oriel Cornerstone). The light intensity was calibrated by a photodiode (UDT 260) at each measured wavelength. The photocurrent was measured by a Keithley 617 electrometer.

■ RESULTS AND DISCUSSION

Synthesis. The synthetic procedures are shown in Scheme 2. Dipyrromethanes were converted to the corresponding dipyrrins by oxidation with *p*-chloranil. Without further purification, the crude product was reacted with a dinuclear precursor $[(\text{p-cymene})RuCl_2]_2$ to form the neutral mono-nuclear complex [(*p*-cymene)Ru(*R*-DP)Cl] (*R*-DP = 3-TDP or TPADP), at which point the product purification was performed. Complexes **1**, **2a**, and **3a** were obtained by refluxing [(*p*-cymene)Ru(*R*-DP)Cl] with bpy or dcmb in MeOH in the presence of $AgNO_3$. Ester derivatives **2a** and **3a** were hydrolyzed to form **2** and **3** by refluxing with Et_3N in a H_2O−DMF solvent mixture for 18 h.

Electronic Structure. To establish the electronic structure of the complexes and aid in the subsequent assignment of optical transitions and electrochemical events, we performed DFT calculations using the B3LYP hybrid functional and TZVP basis set (DZVP for Ru). The energy diagram and selected MOs of **1**, **2**, and **3** are shown in Figure 1.

In **1**, the highest occupied molecular orbital (HOMO), HOMO−1, and HOMO−3 are primarily based on the Ru d orbitals, with a small contribution from the dipyrrinato or bpy π orbitals, while the HOMO−2 is purely dipyrrinato-based (see Table S1 in the Supporting Information). The lowest unoccupied molecular orbital (LUMO) and LUMO+1 correspond to a mixture of dipyrrinato and bpy π* orbitals, while the LUMO+2 and LUMO+3 reside mostly on bpy. The Ru contribution to these four LUMOs ranges from 0.7% for the LUMO to 5.9% for the LUMO+2, indicating a rather weak Ru-to-ligand back-donation in this complex (Table S1).

The addition of electron-withdrawing carboxylic substituents in **2** changes the order of frontier orbital energies by stabilizing the Ru d orbitals and dcbpy π* orbitals. As a result, the dipyrrinato-centered π orbital becomes the HOMO. The mixing between π* orbitals of dcbpy and dipyrrinate is also eliminated, giving rise to bpy-centered LUMO/LUMO+1 and dipyrrinato-centered LUMO+2. The Ru contribution to these three orbitals is 6.5%, 5.4%, and 1.5%, respectively (Table S1). Thus, Ru-to-ligand back-donation in **2** remains weak.

In **3**, the HOMO resides on the TPA moiety, while the order and nature of other frontier MOs are similar to those observed in **2**, suggesting that the meso substituent interacts only weakly with the dipyrrin unit. The latter finding is explained by the lack of coplanarity between the two aromatic fragments.[20]

Optical Spectroscopy. The absorption spectra of **1**, **2**, and **3** are similar (Figure 2) and exhibit three major bands around 300, 450, and beyond 500 nm. The latter band in the spectra of **2** and **3** is red-shifted by 24 nm relative to the analogous band in the spectrum of **1**. The absorption spectra simulated from the TD-DFT calculations reproduce the main features of the experimental spectra quite well (Figure 3) and thus can be used for the assignment of the observed absorption bands (see Table S2 in Supporting Information for the complete list of assigned excitations).

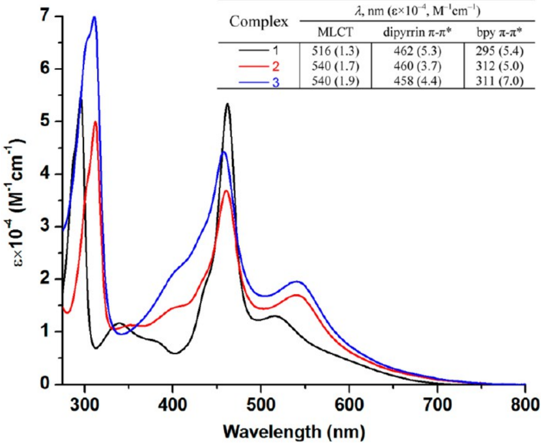

Complex	λ, nm (ε×10^{-4}, M^{-1}cm^{-1})		
	MLCT	dipyrrin π-π*	bpy π-π*
—— 1	516 (1.3)	462 (5.3)	295 (5.4)
—— 2	540 (1.7)	460 (3.7)	312 (5.0)
—— 3	540 (1.9)	458 (4.4)	311 (7.0)

Figure 2. Optical absorption spectra of **1** in MeCN and of **2** and **3** in MeOH at room temperature.

The lower-energy absorption band in Ru(II) polypyridyl complexes can be empirically assigned as the metal-to-ligand charge transfer (MLCT) transition. Indeed, the TD-DFT calculations confirm that the lower-energy band in each complex corresponds to excitations from the Ru d orbitals to the set of three (in **1**) or two (in **2** and **3**) ligand-centered π* orbitals (Figure 1). Since the stabilization of the bpy-centered π* orbitals upon addition of the carboxylic groups exceeds the stabilization of the Ru d orbitals, the MLCT transitions in **2** and **3** have lower energy and hence longer wavelengths. The low-energy band in **3** also contains an admixture of an intraligand charge-transfer (ILCT) excitation from the TPA-centered HOMO to the dipyrrinate-centered LUMO+2. In the case of **2**, the calculated oscillator strength for the excitation from the 3-TDP-centered HOMO to the dcbpy-centered LUMO/LUMO+1 is low, and this transition does not contribute significantly to the optical absorption spectrum.

The intermediate-energy absorption band appears at about the same energy in all three complexes, with the maximum around 460 nm, although the band in **2**, and especially in **3**, is broadened relative to the one observed in **1**. Nevertheless, in all complexes, this band mainly arises from the ligand-to-ligand (LLT) excitations from the dipyrrinato-centered π-orbitals to bpy or dipyrrinato-centered π* orbitals (Table S2). Although the DFT calculations suggest that there is some mixing of LLT and MLCT transitions, they do support the notion that the intermediate-energy band around 460 nm is predominantly composed of LLT excitations and the low-energy band at 540 nm corresponds to MLCT excitations.

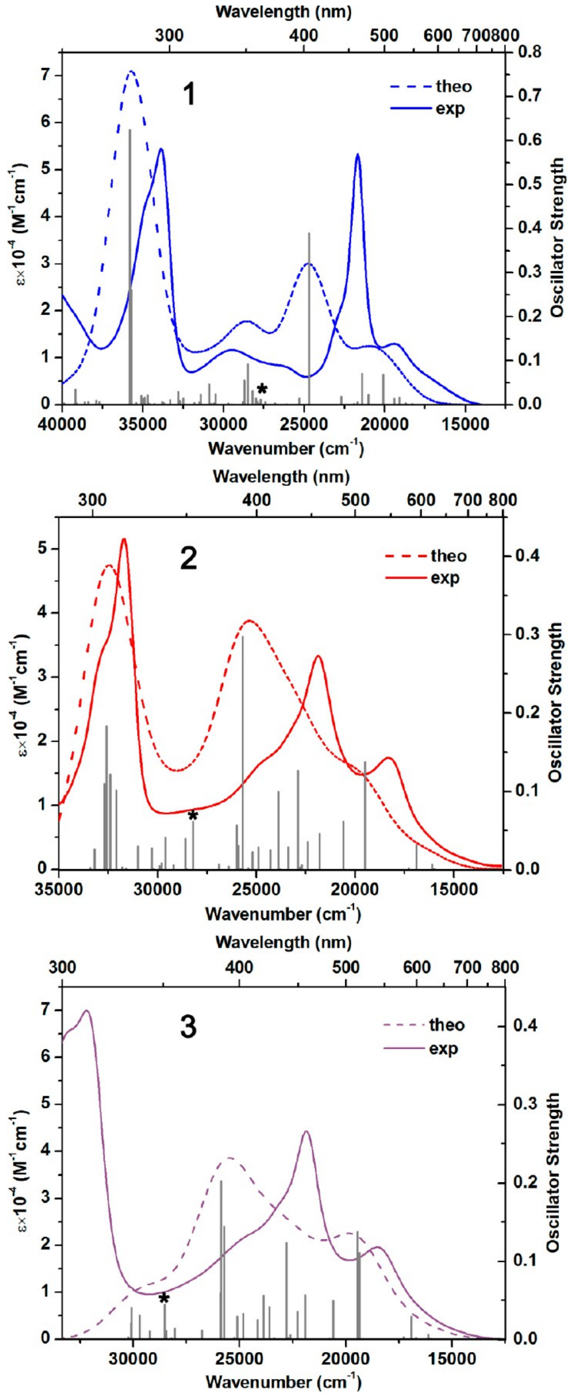

Figure 3. Experimental (solid line) and simulated (dashed line) absorption spectra of **1** (blue), **2** (red), and **3** (purple). The gray bars indicate the energy and oscillator strength of electronic excitations. The asterisk marks the excitation in the simulated spectrum that corresponds to the 400-nm absorption in the experimental spectrum (see the "Transient Absorption Spectroscopy" section for further details).

At room temperature, no measurable photoluminescence signal could be detected in solutions of all three complexes. Nevertheless, at 77 K, a significant photoluminescence was observed from a solution of **3** in EtOH:MeOH glass (4:1 v/v), with the maximum at 760 nm (Figure S1).

Electrochemistry. The cyclic voltammogram (CV) of **1** reveals a quasi-reversible process at $E_{1/2}$ = 0.90 V, attributed to the $Ru^{III/II}$ redox couple, and three quasi-reversible ligand-based redox processes at −1.16, −1.45, and −1.77 V (Figure 4).

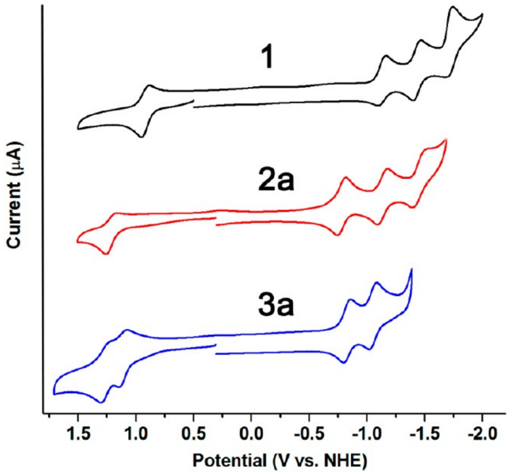

Figure 4. Cyclic voltammograms of **1** (black), **2a** (red), and **3a** (blue) recorded in 0.1 M solutions of $(Bu_4N)PF_6$ in MeCN, CH_2Cl_2, and MeCN, respectively.

Similar to **1**, only one oxidation was observed for **2** at 1.07 V, while the CV of **3** exhibited two successive quasi-reversible processes at $E_{1/2}$ = 1.05 and 1.26 V in DMF electrolyte. The reductions of **2** and **3** were not well resolved. Therefore, the electrochemical behavior of their ester derivatives, **2a** and **3a**, was examined. In comparison to **1**, both **2a** and **3a** were more resistant to oxidation and more susceptible to reduction (Table 1). Such behavior is in accord with the electron-withdrawing nature of the ester substituents, which stabilize both Ru d orbitals and bpy π^* orbitals. Similar to **3**, complex **3a** exhibits two redox events at $E_{1/2}$ = 1.12 and 1.27 V in MeCN solution. To assign these oxidation processes, a CV of the ligand, TPADP, was acquired in MeCN, and one quasi-reversible oxidation at 1.26 V was observed. In addition, a model complex **3b** was prepared, in which the dcbpy ligands were replaced by unsubstituted bpy ligands. In this complex, the second oxidation potential remained unchanged while the first oxidation potential was shifted to much lower value of 0.90 V (Figure S2). This is in agreement with the assignment of the first process to the Ru^{III}/Ru^{II} redox couple, as the absence of the electron-withdrawing ester substituents makes the Ru center more prone to oxidation. In turn, taking into account the coincidence of the second redox potential in **3a** and **3b** and the aforementioned lack of electronic communication between the TPA and dipyrrinate fragments, this redox process can be assigned as the TPA-centered oxidation.

Table 1. Electrochemical Properties of Complexes 1-3, 2a, 3a, and 3b[a]

		half-wave potentials, V		
complex	solvent	$E^{+/0}_{1/2}$	$E^{0/-}_{1/2}$	$E^{-/2-}_{1/2}$
1	MeCN	0.90	−1.16	−1.45
2a	CH_2Cl_2	1.21	−1.78	−1.14
3a	MeCN	1.12, 1.27	−0.83	−1.06
3b	MeCN	0.90 1.27	−1.17	−1.44
2	DMF	1.07		
3	DMF	1.05, 1.26		

[a] The potentials are referenced to NHE.

The excited-state redox potential for **3** was calculated through a free-energy cycle as $E_{1/2}(\mathbf{3}^{+/*}) = E_{1/2}(\mathbf{3}^{+/0}) - \Delta G_{ES}$, where the latter term corresponds to the free energy stored in the excited state. The value ΔG_{ES} = 1.72 eV was abstracted from an intersection of the tangent line drawn on the high-energy side of the 77-K photoluminescence spectrum with the horizontal wavelength axis (Figure S1). Using this value and the electrochemical data for **3**, the value of $E_{1/2}(\mathbf{3}^{+/*})$ was calculated to be −0.67 V vs NHE. Despite our inability to detect photoluminescence from **2**, we anticipate that it has a similar excited-state redox potential based on the similarity of electrochemical and optical properties of **2** and **3**.

Solution-Phase Transient Absorption Spectroscopy. To study the excited-state dynamics, we carried out ultrafast pump−probe experiments on **1**, **2a**, and **3a** in MeCN solutions. The experiments were conducted by exciting sample solution using a 400-nm laser pulse and probing the time-dependent response using a broad bandwidth continuum pulse. Generally, the differential transient absorption spectra of the samples exhibited two major bleach components, one below and the other above 500 nm.

In the case of **1**, excitation by 400-nm light generated ground-state bleaches at 470 and 520 nm (Figure 5a), which corresponded to the ground-state linear absorption bands observed at 462 and 516 nm, respectively. The recovery of the transient bleach signal at 520 nm was best fit using a single-exponential rate law, which yielded a time constant of 4.5 ns. The bleach recovery kinetics of the signal at 470 nm were nonexponential, and required the inclusion of a faster (25 ps) component (Figure 5c). The major recovery channel for the 470-nm bleach was characterized by a time constant of 4(1) ns. The pre-exponential constants of 0.03 and 0.97, respectively, indicate that the slower process made the most significant contribution to the total amplitude of the time-resolved TA signal. In addition, a positive transient signal was observed at 650 nm, indicating excited-state absorption. Placing the results of TA experiments in the context of electronic structure calculations, one can establish that the 400-nm pump resulted in a HOMO−3 → LUMO+3 excitation (Table S2) to the bpy-based π^* orbital (Figure 1). This excited state, most likely, undergoes internal conversion to the next bpy-based π^*-orbital, LUMO+2, followed by vibrational relaxation that delocalizes the electron density over all three ligands, populating nearly degenerate LUMO and LUMO+1. We attribute the 25-ps component in the transient signal to this vibrational relaxation.

Excitation of complexes **2a** and **3a** using 400-nm light also resulted in bleaches at 450 and 550 nm (Figure 5b), corresponding to the LLT and MLCT absorption bands at 460 and 540 nm, respectively. Time-resolved TA measurements, however, revealed significant differences for complexes **2a** and **3a** as compared to **1**. In the case of **3a**, the transient signal monitored at 540 nm exhibited an initial growth with a time constant τ = 2(1) ps, while the signal monitored at 460 nm exhibited an initial recovery at τ = 9(3) ps (Figure 5d). A similar initial growth of the 540-nm signal (τ = 6(2) ps) was observed in the TA spectrum of **2a**. (Unfortunately, we could not follow the evolution of the signal around 460 nm in **2a**, due to a low signal-to-noise ratio, and therefore only complex **3a** will be discussed below.) Both 460- and 540-nm transient

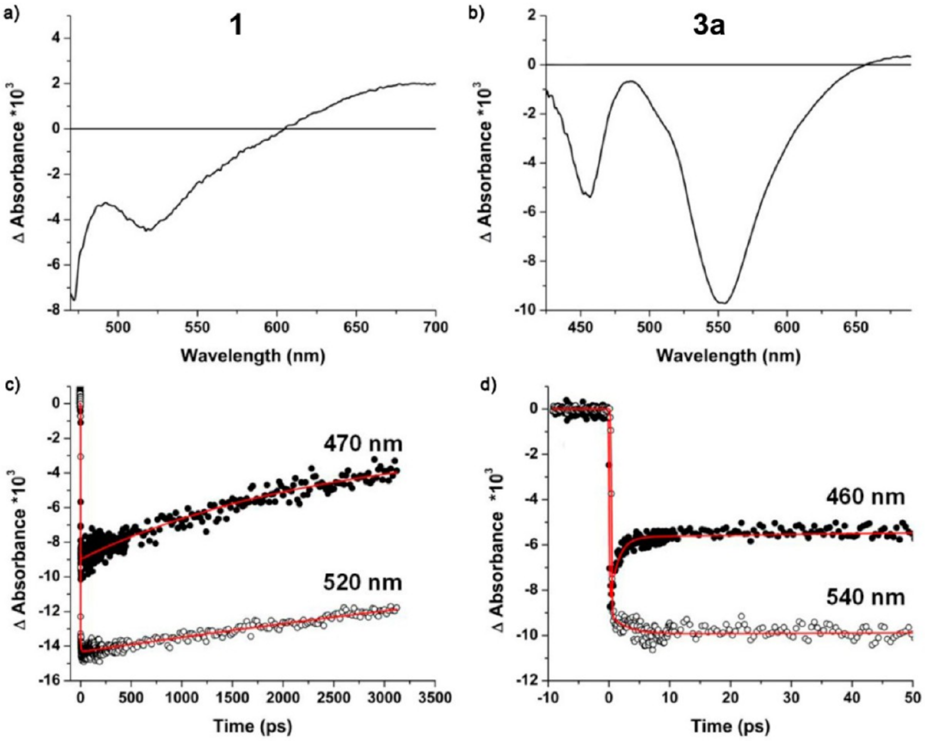

Figure 5. Transient absorption spectra (a and b) and single-wavelength absorption changes monitored at two different wavelengths (c and d) for MeCN solutions of **1** (a and c) and **3a** (b and d), under 400 nm pulsed laser excitation. Overlaid in red on the experimental data are best fits to the decay function described by equation (1).

signals observed for **3a** also showed a longer decay component with a characteristic lifetime of ~13 ns that were within experimental error the same at these observation wavelengths. These states were also independently measured for **3** by nanosecond absorption spectroscopy with a lifetime of 13 ns at −30 °C in ethanol (Figure S3).

The differences in the excited-state dynamics of **3a** and **1** can be rationalized by considering the results of electronic structure calculations and assignments of absorption bands in the spectra of these complexes. In contrast to **1**, the LUMO and LUMO+1 in **3a** are localized π^* orbitals of dcmb and do not exhibit any DP-based character. The 400-nm laser pulse results in promotion of electrons to the dcmb-centered LUMO and LUMO+1 in **3a**, which leads to bleaching of both LLT and MLCT bands. In other words, the bleaches observed at 460 and 540 nm correspond to transitions from the (dcmb/dcmb)-Ru^{II}-DP-TPA ground state to (dcmb/dcmb$^{\bullet-}$)-Ru^{II}-DP^{+}-TPA (LLT) and (dcmb/dcmb$^{\bullet-}$)-Ru^{III}-DP-TPA (MLCT) excited states, respectively (Scheme 3). Importantly, the 540-nm band in **3a** also includes a large contribution from the (dcmb/dcmb$^{\bullet-}$)-Ru^{II}-DP-TPA^{+} charge-separated LLT (CS-LLT) state (Table S2). Considering these excited states, we attribute the initial growth of the 540-nm bleach to the vibrational relaxation process,[40] which decreases the contributions from the Ru → dcmb (MLCT) and TPA → dcmb (CS-LLT) transitions with the concomitant increase in the LLT-type DP → dcmb and DP → DP transitions. Hence, a growth of the 540-nm bleach at the expense of the 460-nm bleach is observed, suggesting energy redistribution from the excitation manifold generated by the LLT absorption to the excited states generated by the MLCT/CS-LLT absorption.

Scheme 3. Energy Level Diagram Illustrating Excited State Dynamics of 3a

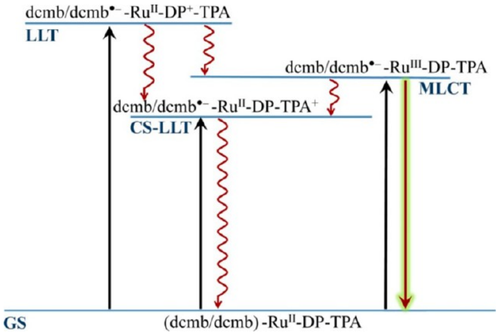

Behavior on TiO$_2$ Surface. Recently, we have reported the first use of Ru dipyrrinates as DSSC sensitizers.[19] We observed that substantial current densities (J_{sc} >10 mA cm^{-2}) could be achieved, but only if the electrolyte contained a large (~1 M) concentration of Li^{+} ions. Nevertheless, the open-circuit voltage remained low (V_{oc} ≈ 0.30 V). Addition of *t*-butylpyridine (TBP), which is a common DSSC electrolyte additive for improving V_{oc}, not only failed to produce the desired change in V_{oc}, but also led to a dramatic decrease in J_{sc}. To understand the origins of such behavior, in the current work we investigated the electron-injection behavior of complexes **2** and **3** deposited on the TiO$_2$ surface.

Dyes **2** and **3** were found to bind strongly to mesoporous nanocrystalline TiO$_2$ thin films. A surface coverage of ~1 × 10^{-7} mol cm^{-2} was obtained after keeping the films for 24 h in a ~3 × 10^{-4} M solution of the dye in EtOH. The films were subsequently immersed into MeCN, and their ground-state absorption spectra were found to be similar to those recorded for free complexes **2** and **3** in solution, although some broadening of the absorption bands was observed. The addition

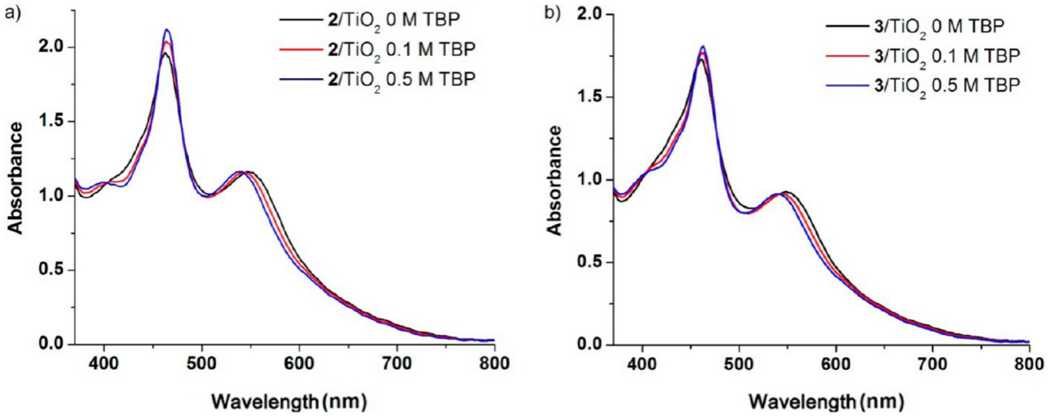

Figure 6. Ground-state absorption spectra of **2** (a) and **3** (b) on the TiO$_2$ surface immersed in a 0.5 M MeCN solution of LiClO$_4$ at variable TBP concentrations.

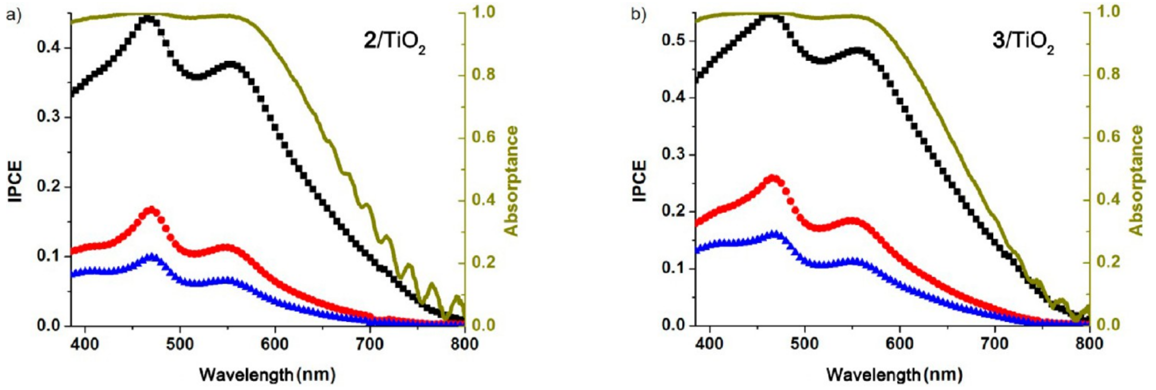

Figure 7. Incident photon-to-current efficiency of **2** (a) and **3** (b) in dye sensitized solar cells with 0.5 M LiI/0.05 M I$_2$ acetonitrile solution and the 0 (black), 0.1 (red), and 0.5 M (blue) TBP content. Also shown in olive green is the absorptance spectrum of the sensitized thin film.

of 0.5 M LiClO$_4$ causes a bathochromic shift of the MLCT band as compared to the spectra recorded on the films immersed in neat MeCN (Figure S4). In contrast, the addition of TBP resulted in a hypsochromic shift of the MLCT band that offset the bathochromic shift induced by the LiClO$_4$ solution (Figure 6). The hypsochromic shift increased from 170 to 300 cm^{-1} when the TBP concentration was increased from 0.1 to 0.5 M. The addition of TBP, however, did not induce a measurable shift of the ligand-based absorption band at intermediate energies but did slightly increase the absorptivity of this band.

The incident photon-to-current efficiency (IPCE) measurements were performed for **2**/TiO$_2$ and **3**/TiO$_2$ under variable excitation wavelengths, with the dye-covered thin films immersed in 0.5 M LiI/0.05 M I$_2$ acetonitrile solution as electrolyte. The IPCE spectra showed two maxima that corresponded to the intermediate-energy LLT band and lower-energy MLCT band (Figure 7), with the maximum observable IPCE values of ~40% for **2** and ~50% for **3**. The addition of 0.1 and 0.5 M TBP led to a dramatic decrease in IPCE by more than 50% and 70%, respectively (Table 2).

Shown with the olive-green line in Figure 7 are the absorptance spectra of **2**/TiO$_2$ and **3**/TiO$_2$ that represent the fraction of incident light absorbed by the sensitized thin films used in these experiments. The fine structure in the absorptance spectra at long wavelengths was attributed to the interference by the thin film. The absorptance at wavelengths below 600 nm was essentially 1 for both sensitizers, indicating quantitative light-harvesting. Therefore, if the injection and the collection yields were quantitative, the photocurrent action spectra would be structureless over this wavelength range and would only be attenuated by reflection losses and the weak absorption of the FTO substrate and the electrolyte. If quantitative injection occurred from the Franck−Condon excited state, the action spectra would also be structureless. Nevertheless, well-defined bands were observed (Figure 7), the energies of which coincide with the absorption maxima of the dyes on the TiO$_2$ film (Figure 6). Interestingly, the 470 nm absoption band was less sensitive to the presence of TBP than

Table 2. IPCE and Comparative Actinometry of Dyes 2 and 3 on the TiO$_2$ Surface

		IPCE[a]		electron injection yield[b]	
dye	concentration of TBP (M)	470 nm	550 nm	416 nm	532 nm
2	0	0.44 (1)	0.38 (1)	1	1
	0.1	0.17 (0.39)	0.11 (0.29)	0.43	0.34
	0.5	0.10 (0.23)	0.07 (0.18)	0.28	0.21
3	0	0.54 (1)	0.48 (1)	1	1
	0.1	0.26 (0.48)	0.18 (0.38)	0.48	0.47
	0.5	0.16 (0.30)	0.11 (0.23)	0.33	0.28

[a] The values were measured as the maxima of the IPCE data that appear at 470 and 550 nm. Shown in parentheses is the ratio of the specific IPCE value to the value measured in the absence of TBP. [b] The wavelengths correspond to the pulsed laser excitations.

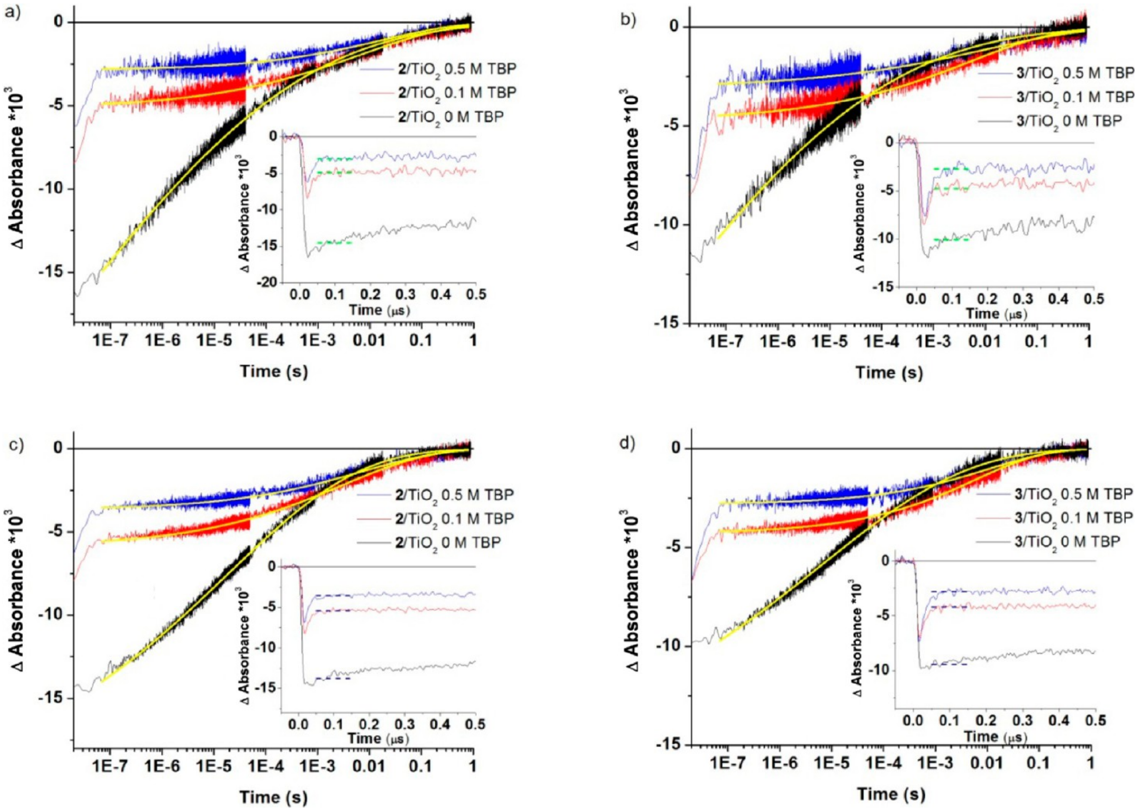

Figure 8. Absorption changes monitored at 542 nm for **2** and **3** anchored to the TiO_2 surface after pulsed-laser excitations with 532 (a and b) and 416 nm (c and d) light. Overlaid on this data are the best fits to the KWW function. The inset displays the first 0.5 μs of data, with dashed lines showing the amplitudes assigned to charge-separated states, which were used to measure the relative injection yield.

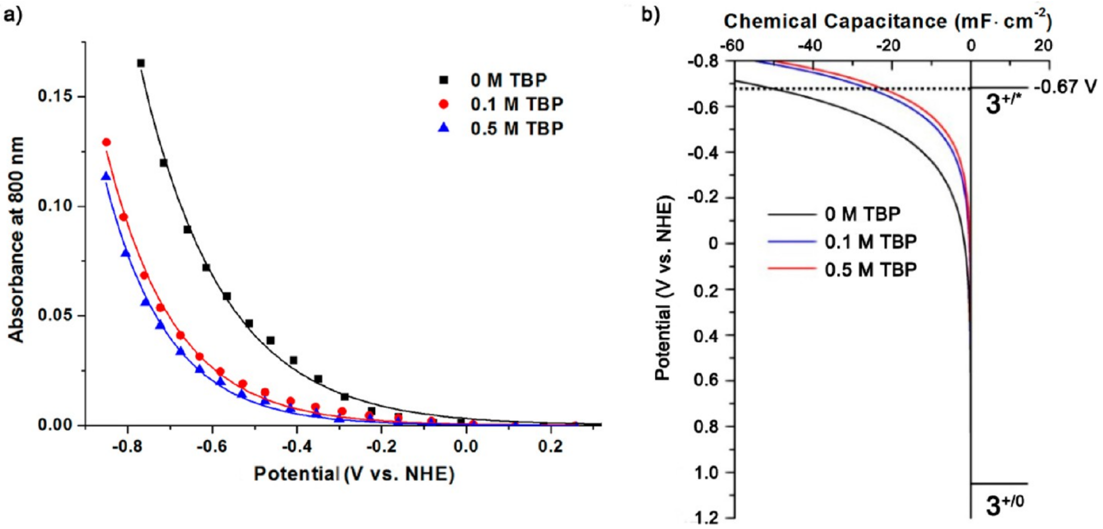

Figure 9. (a) Absorption of dye-free TiO_2 thin-film electrode measured at 800 nm as a function of applied potential (vs NHE) at variable concentrations of TBP. (b) The data from panel a recast as chemical capacitance. Superimposed on these data are the ground- and excited-state redox potentials of dye **3**.

was the lower energy MLCT band. For example, in the case of **3**/TiO_2, the addition of 0.5 M TBP decreased the photocurrent measured at 470 nm by 70% while that at 550 nm was decreased by 77% (Table 2).

To gain further insight into the effect of TBP additive on the photocurrent action, comparative actinometry measurements of **2**/TiO_2 and **3**/TiO_2 were performed in the absence of LiI/I_2 redox mediator. The transient actinometry measurements were performed with a 542 nm observation wavelength that corresponds to an isosbestic point in the presence and absence of TBP (Figure 6) and a 65 ns delay time to exclude possible excited state contributions (Figures S3 and S4). Dyes **2** and **3** thus served as actinometers, and their relative injection yields were taken to be 1 in the absence of TBP. The addition of TBP was found to decrease the injection yield under both 416 and 532 nm excitations (Figure 8 and Table 2). The decreased injection yields are correlated with the appearance of a fast component that is due to the excited state, Figure 8. Importantly, the injection yield achieved with 416 nm excitation was higher than that measured with 532 nm excitation at both TBP concentrations. Similar to the photocurrent action spectra, TBP had a more significant influence on the injection yields when 532 nm excitation was utilized relative to 416 nm. For example, with **3**/TiO_2 the addition of 0.5 M TBP decreased the injection yield by 72% with 532 nm excitation and by only 67% with 416 nm excitation (Table 2).

Kinetics of the absorption signal at 542 nm were nonexponential at all TBP concentrations but could be well fitted to the Kahlraush-William-Watts (KWW) function (eq 2)

$$\Delta\text{Abs} = A\ \exp[-(kt)^{\beta}] \quad (2)$$

The best fits (yellow curves in Figure 8) were obtained with the value of β between 0.08 and 0.35. Higher β values were abstracted from data obtained when TBP was present in the solution.

To rationalize the changes in the IPCE and injection yield, spectroelectrochemistry was utilized to investigate the net effect of TBP on the reduction of TiO_2 in the absence of the dye. Application of a negative external bias to a mesoporous nanocrystalline TiO_2 thin film immersed in a 0.5 M $LiClO_4$/MeCN solution in a standard three-electrode configuration resulted in the well-known absorption spectrum that has been attributed to reduction of TiO_2 acceptor states, abbreviated $TiO_2(e^-)$ herein.[41,42] The characteristic featureless absorption spectrum was observed across the entire visible to near-IR region (Figure S5) and its magnitude at 800 nm was monitored as a function of the applied potential (Figure 9a). The presence of 0.1 M TBP shifted the absorption onset to more negative potentials by approximately 0.2 V, while 0.5 M TBP induced an additional 0.05 V shift. These absorption data were converted to chemical capacitance as was previously described.[43] Superimposing the excited-state reduction potential of **3** on the capacitance data clearly shows that the excited state overlap with the TiO_2 acceptor states decreases as TBP concentration increases. As indicated by the dotted line in Figure 9b, the capacitance decreased by a factor of 2 upon addition of TBP. This drop in capacitance of TiO_2 explains the decrease in the IPCE and injection yield observed in the presence of TBP (Table 2).[44,45]

The IPCE and comparative actinometry clearly demonstrate the decrease in the electron injection yield upon addition of TBP (Figures 7 and 8). Notably, both measurements indicate that the suppression of electron injection into TiO_2 is consistently larger for the 532 nm excitation than for the 416 nm excitation at the same TBP concentration (Table 2). These observations suggest more efficient excited state injection from the 460-nm absorption, which could be explained by electron injection from the upper excited states. This so-called hot injection was also previously demonstrated for some other dyes.[46−48] Nevertheless, it must be noted that vibrational relaxation, which is described by a time constant of 2 ps in solution of **3**, can kinetically compete with the hot electron-injection process. The overall consequence is that the electron injection yield decreases at all excitation wavelengths upon TBP addition, but less so for the higher-energy excitations. The acceptor states shift in energy toward the vacuum level upon the addition of TBP (Figure 9b). This results in a smaller overlap of the excited state with the TiO_2 acceptor levels that in turn decreases the electron injection yield.

■ CONCLUSIONS

The electrochemical and photophysical characteristics of Ru dipyrrinates **2** and **3** render them viable candidates for DSSC sensitization. The TD-DFT calculations indicate the preferential localization of the excited electron on the anchoring H_2dcbpy ligands, which results in a favorable scenario for photoinduced electron injection into TiO_2. Nevertheless, as was demonstrated in our earlier contribution, the performance of Ru dipyrrinates as DSSC sensitizers is subpar to their excellent light-harvesting properties.[19] The studies of the excited-state and electron-transfer dynamics reveal that these excited states are weak photoreductants that do not transfer electrons to TiO_2 efficiently under many experimental conditions. This was particularly evident when *tert*-butyl pyridine (TBP) was present and the injection yields measured spectroscopically or inferred from photocurrent action spectra decreased markedly. Importantly, the injection yields with ligand-localized excitation were less sensitive to the TBP concentration than the yields obtained with the lower energy MLCT excitation. This suggests that dyes **2** and **3** are capable of hot injection from upper ligand-localized excited states.

The most obvious target for improving the performance of Ru(II) dipyrrinates as DSSC dyes is to make them stronger photoreductants. This goal can be achieved by introducing electron-donating substituents into the pyrrolic rings of the dipyrrinate ligand or by substituting one of the anchoring H_2dcbpy ligand with a bpy that contains electron-donating groups. We are currently exploring both of these approaches, and the properties and DSSC performance of the modified Ru dipyrrinate dyes will be reported in due course.

■ ASSOCIATED CONTENT

Ⓢ Supporting Information

Cyclic voltammogram of **3b**, detailed electronic transition assignments for **1**−**3**, photoluminescence of **3** at 77 K, difference absorption of **3** in EtOH, and ground-state absorption spectra of **2** and **3** on TiO_2. This material is available free of charge via the Internet at http://pubs.acs.org.

■ AUTHOR INFORMATION

Notes

The authors declare no competing financial interest.

■ ACKNOWLEDGMENTS

M.S. and G.L. acknowledge the Council for Research and Creativity at Florida State University for the support of this project. The work of G.J.M and K.H. was funded by the Division of Chemical Sciences, Geosciences, and Biosciences, Office of Basic Energy Sciences of the U.S. Department of Energy through Grant DE-FG02-96ER14662. S.I.G. thanks the Centre for Catalysis Research and Innovation (CCRI) for funding and computing resources. Some of this material was based on work supported by the U.S. Air Force Office of Scientific Research under AFOSR award FA9550-10-1-0300 to K.L.K.

■ REFERENCES

(1) Grätzel, M. Solar Energy Conversion by Dye-Sensitized Photovoltaic Cells. *Inorg. Chem.* **2005**, *44*, 6841−6851.

(2) O'Regan, B.; Grätzel, M. A Low-Cost, High-Efficiency Solar Cell Based on Dye-Sensitized Colloidal Titanium Dioxide Films. *Nature* **1991**, *353*, 737−740.

(3) Vlachopoulos, N.; Liska, P.; Augustynski, J.; Grätzel, M. Very Efficient Visible Light Energy Harvesting and Conversion by Spectral Sensitization of High Surface Area Polycrystalline Titanium Dioxide Films. *J. Am. Chem. Soc.* **1988**, *110*, 1216−1220.

(4) Hagfeldt, A.; Boschloo, G.; Sun, L. C.; Kloo, L.; Pettersson, H. Dye-Sensitized Solar Cells. *Chem. Rev.* **2010**, *110*, 6595−6663.

(5) Robertson, N. Optimizing Dyes for Dye-Sensitized Solar Cells. *Angew. Chem., Int. Ed.* **2006**, *45*, 2338−2345.

(6) Nazeeruddin, M. K.; Kay, A.; Rodicio, I.; Humphrybaker, R.; Muller, E.; Liska, P.; Vlachopoulos, N.; Grätzel, M. Conversion of Light to Electricity by *cis*-X_2Bis(2,2′-bipyridyl-4,4′-dicarboxylate)-ruthenium(II) Charge-Transfer Sensitizers ($X = Cl^-$, Br^-, I^-, CN^-, and SCN^-) on Nanocrystalline TiO_2 Electrodes. *J. Am. Chem. Soc.* **1993**, *115*, 6382−6390.

(7) Nazeeruddin, M. K.; Zakeeruddin, S. M.; Humphry−Baker, R.; Jirousek, M.; Liska, P.; Vlachopoulos, N.; Shklover, V.; Fischer, C. H.; Grätzel, M. Acid−Base Equilibria of (2,2′-Bipyridyl-4,4′-dicarboxylic acid)ruthenium(II) Complexes and the Effect of Protonation on Charge-Transfer Sensitization of Nanocrystalline Titania. *Inorg. Chem.* **1999**, *38*, 6298−6305.

(8) Nazeeruddin, M. K.; et al. Engineering of Efficient Panchromatic Sensitizers for Nanocrystalline TiO_2−Based Solar Cells. *J. Am. Chem. Soc.* **2001**, *123*, 1613−1624.

(9) Ardo, S.; Meyer, G. J. Photodriven Heterogeneous Charge Transfer with Transition−Metal Compounds Anchored to TiO_2 Semiconductor Surfaces. *Chem. Soc. Rev.* **2009**, *38*, 115−164.

(10) Bessho, T.; Yoneda, E.; Yum, J. H.; Guglielmi, M.; Tavernelli, I.; Imai, H.; Rothlisberger, U.; Nazeeruddin, M. K.; Grätzel, M. New Paradigm in Molecular Engineering of Sensitizers for Solar Cell Applications. *J. Am. Chem. Soc.* **2009**, *131*, 5930−5934.

(11) Bomben, P. G.; Robson, K. C. D.; Sedach, P. A.; Berlinguette, C. P. On the Viability of Cyclometalated Ru(II) Complexes for Light-Harvesting Applications. *Inorg. Chem.* **2009**, *48*, 9631−9643.

(12) Bomben, P. G.; Gordon, T. J.; Schott, E.; Berlinguette, C. P. A Trisheteroleptic Cyclometalated Ru^{II} Sensitizer That Enables High Power Output in a Dye-Sensitized Solar Cell. *Angew. Chem., Int. Ed.* **2011**, *50*, 10682−10685.

(13) Wu, K. L.; Hsu, H. C.; Chen, K.; Chi, Y.; Chung, M. W.; Liu, W. H.; Chou, P. T. Development of Thiocyanate-Free, Charge-Neutral Ru(II) Sensitizers for Dye-Sensitized Solar Cells. *Chem. Commun.* **2010**, *46*, 5124−5126.

(14) Chou, C. C.; Wu, K. L.; Chi, Y.; Hu, W. P.; Yu, S. J.; Lee, G. H.; Lin, C. L.; Chou, P. T. Ruthenium(II) Sensitizers with Heteroleptic Tridentate Chelates for Dye-Sensitized Solar Cells. *Angew. Chem., Int. Ed.* **2011**, *50*, 2054−2058.

(15) Phuong, N. T.; Andersen, A. R.; Skou, E. M.; Lund, T. Dye Stability and Performances of Dye-Sensitized Solar Cells with Different Nitrogen Additives at Elevated Temperatures: Can Sterically Hindered Pyridines Prevent Dye Degradation? *Solar Energy Mater. Solar Cells* **2010**, *94*, 1582−1590.

(16) Bomben, P. G.; Gordon, T. J.; Schott, E.; Berlinguette, C. P. A Trisheteroleptic Cyclometalated Ru^{II} Sensitizer That Enables High Power Output in a Dye-Sensitized Solar Cell. *Angew. Chem., Int. Ed.* **2011**, *50*, 10682−10685.

(17) Robson, K. C. D.; Koivisto, B. D.; Yella, A.; Sporinova, B.; Nazeeruddin, M. K.; Baumgartner, T.; Grätzel, M.; Berlinguette, C. P. Design and Development of Functionalized Cyclometalated Ruthenium Chromophores for Light-Harvesting Applications. *Inorg. Chem.* **2011**, *50*, 5494−5508.

(18) Chou, C. C.; Wu, K. L.; Chi, Y.; Hu, W. P.; Yu, S. J.; Lee, G. H.; Lin, C. L.; Chou, P. T. Ruthenium(II) Sensitizers with Heteroleptic Tridentate Chelates for Dye-Sensitized Solar Cells. *Angew. Chem., Int. Ed.* **2011**, *50*, 2054−2058.

(19) Li, G.; Bomben, P. G.; Robson, K. C. D.; Gorelsky, S. I.; Berlinguette, C. P.; Shatruk, M. Ru Complexes of Thienyl-Functionalized Dipyrrins as NCS-Free Sensitizers for the Dye−-Sensitized Solar Cell. *Chem. Commun.* **2012**, *48*, 8790−8792.

(20) Li, G.; Ray, L.; Glass, E. N.; Kovnir, K.; Khoroshutin, A.; Gorelsky, S. I.; Shatruk, M. Synthesis of Panchromatic Ru(II) Thienyl−Dipyrrin Complexes and Evaluation of Their Light-Harvesting Capacity. *Inorg. Chem.* **2012**, *51*, 1614−1624.

(21) Wood, T. E.; Thompson, A. Advances in the Chemistry of Dipyrrins and Their Complexes. *Chem. Rev.* **2007**, *107*, 1831−1861.

(22) Smalley, S. J.; Waterland, M. R.; Telfer, S. G. Heteroleptic Dipyrrin/Bipyridine Complexes of Ruthenium(II). *Inorg. Chem.* **2009**, *48*, 13−15.

(23) McLean, T. M.; Cleland, D. M.; Lind, S. J.; Gordon, K. C.; Telfer, S. G.; Waterland, M. R. Strongly Absorbing $\pi-\pi^*$ States in Heteroleptic Dipyrrin/2,2′-Bipyridine Ruthenium Complexes: Excited−State Dynamics from Resonance Raman Spectroscopy. *Chem. Asian J.* **2010**, *5*, 2036−2046.

(24) Fulmer, G. R.; Miller, A. J. M.; Sherden, N. H.; Gottlieb, H. E.; Nudelman, A.; Stoltz, B. M.; Bercaw, J. E.; Goldberg, K. I. NMR Chemical Shifts of Trace Impurities: Common Laboratory Solvents, Organics, and Gases in Deuterated Solvents Relevant to the Organometallic Chemist. *Organometallics* **2010**, *29*, 2176−2179.

(25) Pavlishchuk, V. V.; Addison, A. W. Conversion Constants for Redox Potentials Measured Versus Different Reference Electrodes in Acetonitrile Solutions at 25 Degree. *Inorg. Chim. Acta* **2000**, *298*, 97−102.

(26) Maiti, N.; Lee, J.; Do, Y.; Shin, H.; Churchill, D. Synthesis and Structures of Thienyl−Substituted 5−Dipyrromethane Isomers. *J. Chem. Crystallogr.* **2005**, *35*, 949−955.

(27) Wiederholt, K.; McLaughlin, L. W. A 2,2′-Bipyridine Ligand for Incorporation into Oligodeoxynucleotides: Synthesis, Stability and Fluorescence Properties of Ruthenium−DNA Complexes. *Nucl. Acids. Res.* **1999**, *27*, 2487−2493.

(28) Bennett, M. A.; Huang, T. N.; Matheson, T. W.; Smith, A. K.; Ittel, S.; Nickerson, W., 16. (η^6-Hexamethylbenzene)ruthenium Complexes. *Inorganic Syntheses*; John Wiley & Sons, Inc.: New York, 2007; pp 74−78.

(29) Hrobáriková, V.; Hrobárik, P.; Gajdoš, P.; Fitilis, I.; Fakis, M.; Persephonis, P.; Zahradník, P. Benzothiazole-Based Fluorophores of Donor-π-Acceptor-π-Donor Type Displaying High Two-Photon Absorption. *J. Org. Chem.* **2010**, *75*, 3053−3068.

(30) Frisch, M. J. et al. *Gaussian 09*, revision A.02; Gaussian Inc.: Wallingford, CT, 2009.

(31) Lee, C.; Yang, W.; Parr, R. G. Development of the Colle−Salvetti Correlation−Energy Formula into a Functional of the Electron Density. *Phys. Rev. B* **1988**, *37*, 785−789.

(32) Becke, A. D. Density-Functional Exchange-Energy Approximation with Correct Asymptotic Behavior. *Phys. Rev. A* **1988**, *38*, 3098−3100.

(33) Godbout, N.; Salahub, D. R.; Andzelm, J.; Wimmer, E. Optimization of Gaussian-Type Basis-Sets for Local Spin-Density Functional Calculations. Part I. Boron through Neon, Optimization Technique and Validation. *Can. J. Chem.* **1992**, *70*, 560−571.

(34) Schafer, A.; Huber, C.; Ahlrichs, R. Fully Optimized Contracted Gaussian Basis Sets of Triple Zeta Valence Quality for Atoms Li to Kr. *J. Chem. Phys.* **1994**, *100*, 5829−5835.

(35) Gorelsky, S. I.; Lever, A. B. P. Electronic Structure and Spectra of Ruthenium Diimine Complexes by Density Functional Theory and INDO/S. Comparison of the Two Methods. *J. Organomet. Chem.* **2001**, *635*, 187−196.

(36) Gorelsky, S. I. *SWizard program*; University of Ottawa: Ottawa, Canada, 2010; http://www.sg-chem.net/.

(37) Gorelsky, S. I. *AOMix: Program for molecular orbital analysis*, version 6.5; University of Ottawa: Ottawa, Canada, 2011; http://www.sg-chem.net/.

(38) Dowgiallo, A. M.; Knappenberger, K. L. Ultrafast Electron−Phonon Coupling in Hollow Gold Nanospheres. *Phys. Chem. Chem. Phys.* **2011**, *13*, 21585−21592.

(39) Argazzi, R.; Bignozzi, C. A.; Heimer, T. A.; Castellano, F. N.; Meyer, G. J. Enhanced Spectral Sensitivity from Ruthenium(II)

Polypyridyl Based Photovoltaic Devices. *Inorg. Chem.* **1994**, *33*, 5741−5749.

(40) Damrauer, N. H.; McCusker, J. K. Ultrafast Dynamics in the Metal-to-Ligand Charge Transfer Excited−State Evolution of [Ru(4,4′-diphenyl-2,2′-bipyridine)$_3$]$^{2+}$. *J. Phys. Chem. A* **1999**, *103*, 8440−8446.

(41) Boschloo, G.; Fitzmaurice, D. Electron Accumulation in Nanostructured TiO_2 (Anatase) Electrodes. *J. Phys. Chem. B* **1999**, *103*, 7860−7868.

(42) O'Regan, B.; Grätzel, M.; Fitzmaurice, D. Optical Electrochemistry I: Steady−State Spectroscopy of Conduction-Band Electrons in a Metal Oxide Semiconductor Electrode. *Chem. Phys. Lett.* **1991**, *183*, 89−93.

(43) Bisquert, J.; Fabregat-Santiago, F.; Mora-Seró, I.; Garcia-Belmonte, G.; Barea, E. M.; Palomares, E. A Review of Recent Results on Electrochemical Determination of the Density of Electronic States of Nanostructured Metal−Oxide Semiconductors and Organic Hole Conductors. *Inorg. Chim. Acta* **2008**, *361*, 684−698.

(44) Yanagida, M.; Yamaguchi, T.; Kurashige, M.; Hara, K.; Katoh, R.; Sugihara, H.; Arakawa, H. Panchromatic Sensitization of Nanocrystalline TiO_2 with *cis*-Bis(4-Carboxy-2-[2′-(4′-Carboxypyridyl)]Quinoline)Bis(Thiocyanato-*N*)Ruthenium(II). *Inorg. Chem.* **2003**, *42*, 7921−7931.

(45) Johansson, P. G.; Rowley, J. G.; Taheri, A.; Meyer, G. J.; Singh, S. P.; Islam, A.; Han, L. Long-Wavelength Sensitization of TiO_2 by Ruthenium Diimine Compounds with Low-Lying π^* Orbitals. *Langmuir* **2011**, *27*, 14522−14531.

(46) Ferrere, S.; Gregg, B. A. Photosensitization of TiO_2 by [Fe^{II}(2,2′-Bipyridine-4,4′-dicarboxylic acid)$_2$(CN)$_2$]: Band Selective Electron Injection from Ultra-Short-Lived Excited States. *J. Am. Chem. Soc.* **1998**, *120*, 843−844.

(47) Heimer, T. A.; Heilweil, E. J.; Bignozzi, C. A.; Meyer, G. J. Electron Injection, Recombination, and Halide Oxidation Dynamics at Dye-Sensitized Metal Oxide Interfaces. *J. Phys. Chem. A* **2000**, *104*, 4256−4262.

(48) Liu, F.; Meyer, G. J. Excited State Interfacial Electron Transfer from a Compound with a Single Pyridine Ligand. *Inorg. Chem.* **2003**, *42*, 7351−7353.